Taylor & Francis
Taylor & Francis Group

Automatika

Journal for Control, Measurement, Electronics, Computing and Communications

ISSN: (Print) (Online) Journal homepage: https://www.tandfonline.com/loi/taut20

Optimization of bias current coefficient in the fault-tolerance of active magnetic bearings based on the redundant structure parameters

Xin Cheng, Shuai Deng, Baixin Cheng, Meiqian Lu & Rougang Zhou

To cite this article: Xin Cheng, Shuai Deng, Baixin Cheng, Meiqian Lu & Rougang Zhou (2020) Optimization of bias current coefficient in the fault-tolerance of active magnetic bearings based on the redundant structure parameters, Automatika, 61:4, 602-613, DOI: 10.1080/00051144.2020.1806012

To link to this article: https://doi.org/10.1080/00051144.2020.1806012

Published online: 24 Aug 2020.

AUTOMATIKA
2020, VOL. 61, NO. 4, 602–613
https://doi.org/10.1080/00051144.2020.1806012

REGULAR PAPER

OPEN ACCESS Check for updates

Optimization of bias current coefficient in the fault-tolerance of active magnetic bearings based on the redundant structure parameters

Xin Cheng[a,b], Shuai Deng[a], Baixin Cheng[a], Meiqian Lu[a] and Rougang Zhou[c]

[a]School of Mechanical & Electronic Engineering, Wuhan University of Technology, Wuhan, People's Republic of China; [b]Hubei Provincial Engineering Technology Research Center for Magnetic Suspension, Wuhan University of Technology, Wuhan, People's Republic of China; [c]School of Mechanical Engineering, Hangzhou Dianzi University, Hangzhou, People's Republic of China

ABSTRACT

To improve the reliability of magnetic bearings, the redundant structures are usually designed to provide the desired bearing characteristics continually by the reconfiguration of the remaining structures when some components fail. Bias current coefficient is one of the key coefficients in the fault-tolerant control (FTC) of magnetically levitated bearings, and its inappropriate value will result in the failure of providing the desired bearing force due to saturation constraints. This paper presents optimization approaches of the bias current coefficient based on the redundant structure parameters. By analysing the range of the bias current coefficient under saturation constraints mathematically, the existence of the optimal solution has been proved, and the model of the electromagnetic force (EMF), load current and the bias current coefficient has been established in this paper. In addition, algorithms to find the optimal solution has been designed for two kinds of optimization objectives, respectively, in FTC of magnetic bearings. Numerical verifications prove the effectiveness and the versatility of the proposed approaches in the different structures.

ARTICLE HISTORY
Received 18 June 2020
Accepted 23 July 2020

KEYWORDS
Magnetic bearings; bias current coefficient; optimization; fault-tolerance

1. Introduction

Magnetic bearings, support the rotors by electromagnetic force, with the advantages of no lubrication, no mechanical friction, and controllable support characteristics [1,2], are widely used in high-performance equipment such as aero-engines, energy storage flywheels, nuclear turbine power generation equipment, etc., [1–3]. The basic control theory of magnetic bearings is based on the bias current linearization at the equilibrium position, namely, by the displacement-force coefficient and the current-force coefficient, electromagnetic force is linearized [2].

The faults incorporated in magnetic bearings can be divided into 3 types: controller, sensors and actuators. The hot standby configurations of the controller or sensors are the common way to deal with the corresponding faults in the magnetic bearing system [4,5], or more advanced hardware redundancy protocol for achieving high reliability, triple modular redundancy (TMR) [6,7], can be considered in some researches. However, there is special consideration of the faults in the actuators. Because of the requirement of high efficiency in magnetic bearings, it is practically impossible to design some hot standby actuators prepared to replace the failed ones only. Moreover, there is a symmetry constraint on the stator structure [8], the short circuit, break or partial insulation damages in the electromagnetic coils will cause the unexpected EMF, which is defined as the actuator fault [5] and will destroy the original symmetry of the bearing structure, leading to the failure of bearing system and serious impacts [9].

Unlike hot standby configurations, another analytical redundancy design was introduced in [8,10] and can effectively improve the reliability of magnetically levitated bearings. The failed actuators will be isolated and the remaining parts will be continually used and reconfigured to support the magnetically levitated rotor. Similarly, the linearization of EMF generated by redundant supporting structure in magnetic bearings is an important foundation for the realization of FTC, and relevant researches basically follow this idea. Eric et al. [10] proposed the fault-tolerance of magnetic bearings by generalized bias current linearization, in which, the magnetic flux lost due to failed actuator can be compensated by the current distribution, and a linear relationship between the EMF and the controlled current can be derived. Na and Palazzolo [11] optimized the FTC of magnetic bearing and put forward an approach for optimal selection of the current distribution matrix by Lagrange multiplier approach. Moreover, the corresponding experimental verification was performed in their flexible rotor platform [12] to bear the rotor after the failure of an actuator. Subsequently, Ming-Hsiu

CONTACT Rougang Zhou zhourg@hdu.edu.cn School of Mechanical Engineering, Hangzhou Dianzi University, Hangzhou 310000, People's Republic of China

Li [13] studied the magnetic circuit coupled actuator structure and extended the theory to magnetic bearings of composite structure with radial and axial structure. D. Noh et al. [14] experimentally verified the feasibility of such bias current linearization theory based on the molecular magnetic vacuum pump. In addition, in order to effectively compensate for the model error of the linearization method, Meeker and Maslen [15] estimated factors such as magnetic leakage and edge and eddy current effects and established a more accurate magnetic bearing model. Na and Palazzolo [16] calculated the reluctance of ferromagnetic material path and modelling error due to magnetic leakage. The edge effects were replaced by means of a simple compensation coefficient.

The aforementioned researches have already presented a basic theoretical framework in the fault-tolerance of magnetic bearings, however, the following fields need to be concerned. (1) Analysis of the fault-tolerant control system (FTCS) model in magnetic bearings. Arslan A-A. and Khalid M-H. presented a comprehensive state-of-the-art review of FTCS with the latest advances and applications in [17]. Active FTCS (AFTCS) consists of Fault Detection and Isolation (FDI) module [18], a reconfiguration mechanism and a reconfigurable controller [19,20]. Especially, linear regression-based observer model can be used in the fault detection and isolation unit for fault detection, isolation and reconfiguration in the AFTCS [21] to improve the system robustness. Passive FTCS (PFTCS) has no FDI unit and no controller reconfiguration. Rather, the controller works in offline mode in both normal and abnormal conditions with predefined parameters that mask the faulty readings from the components [17]. Hybrid fault-tolerant control system possesses properties of both active fault-tolerant control system and passive fault-tolerant control system. A hybrid fault-tolerant control system was proposed in [22] for air–fuel ratio control of internal combustion gasoline engines based on Kalman filters and triple modular redundancy. (2) Be similar with the common magnetic bearings, the ones with analytical redundancy design have the requirements to linearize the EMF based on a necessary bias design. In order to optimize the EMF output in the FTC of magnetically levitated bearings, Na and Palazzolo [23] designed an optimal selection scheme of current distribution matrix based on the load current limitations and necessary linearization conditions, to lower the load current, compared with the current in [10]. Bias current coefficient is one of the key coefficients in the general current linearization theory [11,14,24,25]. Na et al. [11] gets a certain optimization result by selecting the central intensity of magnetic field as a bias current coefficient. Cheng X. et al. [25] established a FTC model, and through the numerical verification, they pointed out that inappropriate choice of bias current coefficient would cause the failure of generating the desired EMF due to the saturation of the load current or the magnetic field. However, based on what we know, there is no further research about how to find the optimized bias current coefficient in FTCS for magnetic bearings.

Our contribution in this paper is an optimization approach of bias current coefficient based on the redundant supporting structure parameters. We define two kinds of optimization objectives, (1) maximum electromagnetic force under the same structure and saturation constraints and (2) minim intensity of magnetic field under the same structure and EMF output. By analysing the range of the bias current coefficient under saturation constraints mathematically, the existence of the optimal solution has been proved, and the optimization algorithms have been designed to find the optimal solution of bias current coefficient. Numerical verifications prove the efficiency and the versatility of the proposed approaches in different structures. The topic of this paper is not the FTC algorithm but the optimization of bias current coefficient in FTC. The implementation and performance verification of FTC in magnetic bearings can be found in [10–12,14,21].

Further contents of the paper are organized as follows: Section 2 describes the structure parameters in fault-tolerance of magnetic bearings. Section 3 provides the mathematical proofs and Section 4 discusses the optimization algorithms of the optimal bias current coefficient. The numerical verification is in Section 5. The conclusion is presented in the last section with future directions.

2. Structure parameters in the fault-tolerance of magnetic bearing

Figure 1 illustrates the redundant structure and magnetic circuit of radial magnetic bearing with n poles [10]. Relying on the coupled magnetic circuit between adjacent magnetic poles by the magnetic yoke, the loss of magnetic flux caused by the failures of some actuators can be compensated to implement the fault-tolerance. The idea relieves the symmetry constraint on stator structure.

The magnetic circuit equation is [10],

$$R_j\Phi_j - R_{j+1}\Phi_{j+1} = N_jI_j - N_{j+1}I_{j+1} \tag{1}$$

where, R_j and Φ_j are reluctance and magnetic flux of the jth pole, respectively; N_j and I_j are the number of the coil windings and the current of the jth pole, respectively. $g(x,y)_j$, A_j and μ_0 are the gap and area of jth pole, and vacuum magnetic permeability, respectively. One can write

$$R_j = \frac{g(x,y)_j}{\mu_0 A_j} \tag{2}$$

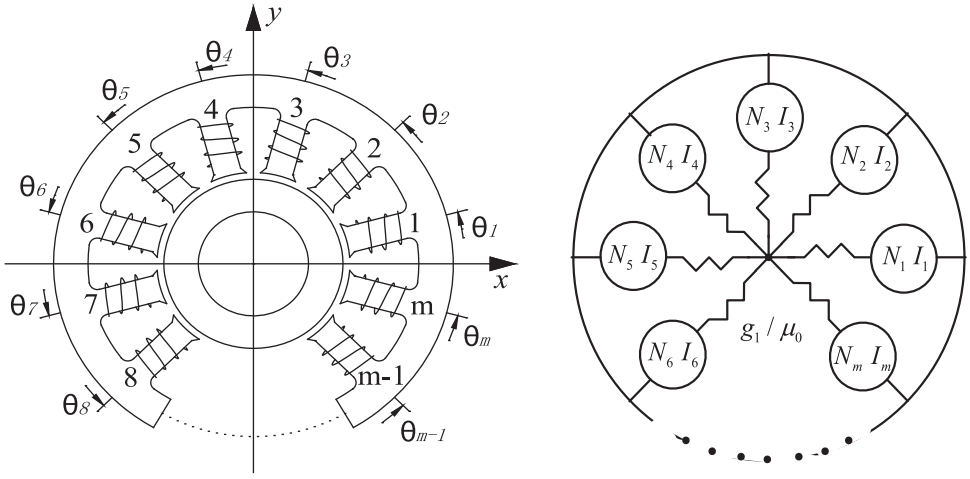

Figure 1. Redundant structure (left), and magnetic circuit (right) of radial magnetic bearing.

Define

$$\boldsymbol{\Phi} = \begin{bmatrix} \Phi_1 & \Phi_2 & \cdots & \Phi_j & \cdots & \Phi_n \end{bmatrix}^T \tag{3}$$

$$\boldsymbol{I} = \begin{bmatrix} I_1 & I_2 & \cdots & I_j & \cdots & I_n \end{bmatrix}^T \tag{4}$$

$$\boldsymbol{R} = \begin{bmatrix} R_1 & -R_2 & 0 & \cdots & 0 \\ 0 & R_2 & -R_3 & \ddots & \vdots \\ \vdots & 0 & \ddots & \ddots & 0 \\ 0 & \cdots & 0 & R_{n-1} & R_n \\ 1 & 1 & \cdots & 1 & 1 \end{bmatrix} \tag{5}$$

$$\boldsymbol{N} = \begin{bmatrix} N_1 & -N_2 & 0 & \cdots & 0 \\ 0 & N_2 & -N_3 & \ddots & \vdots \\ \vdots & 0 & \ddots & \ddots & 0 \\ 0 & \cdots & 0 & N_{n-1} & N_n \\ 0 & 0 & \cdots & 0 & 0 \end{bmatrix} \tag{6}$$

Then, the equation of coupling magnetic circuit is as following [10]

$$\boldsymbol{R\Phi} = \boldsymbol{NI} \tag{7}$$

Note $\Phi_j = B_j A_j$, where B_j is the air gap magnetic field intensity of the jth pole. We define $A_j = A$, and

$$\boldsymbol{B} = \begin{bmatrix} B_1 & B_2 & \cdots & B_j & \cdots & B_n \end{bmatrix}^T \tag{8}$$

$\boldsymbol{B}$ can be described as

$$\boldsymbol{B} = \boldsymbol{A^{-1}R^{-1}NI} \tag{9}$$

In the Equation (9), A represents the diagonal matrix of the magnetic pole area. Fx and Fy are the resultant forces of the EMF in the x and y directions, respectively. Then one can write

$$\begin{cases} F_x = \frac{A}{2\mu_0} \boldsymbol{B^T D_x B} \\ F_y = \frac{A}{2\mu_0} \boldsymbol{B^T D_y B} \\ \boldsymbol{D_x} = \mathrm{diag}\begin{bmatrix} \cos\theta_1 & \cos\theta_2 & \cdots & \cos\theta_n \end{bmatrix} \\ \boldsymbol{D_y} = \mathrm{diag}\begin{bmatrix} \sin\theta_1 & \sin\theta_2 & \cdots & \sin\theta_n \end{bmatrix} \end{cases} \tag{10}$$

It can be seen that even if an electromagnetic coil fails, the corresponding magneto-motive force is 0, but the Equation (10) can still hold, namely, the reconfiguration of the supporting force is realized by the compensation of magnetic flux. We define

$$\boldsymbol{V} = \boldsymbol{A^{-1}R^{-1}N} \tag{11}$$

The diagonal matrix $\boldsymbol{K}$ is introduced to describe the state of the electromagnetic coil. If a coil fails, the corresponding diagonal element is 0.

$$\boldsymbol{K} = diag\underbrace{\begin{bmatrix} 1 & 1 & \cdots & 1 \end{bmatrix}}_{n} \tag{12}$$

Then, Fx and Fy can be described as [10]

$$\begin{cases} F_x = \frac{A}{2\mu_0} \boldsymbol{I^T K^T V^T D_x V K I} \\ F_y = \frac{A}{2\mu_0} \boldsymbol{I^T K^T V^T D_y V K I} \end{cases} \tag{13}$$

Current vector is defined as $\boldsymbol{I_C} = \begin{bmatrix} C_0 & i_x & i_y \end{bmatrix}^T$, where C_0 is the bias current coefficient, i_x and i_y are the control currents in the x and y directions, respectively. Current distribution matrix $\boldsymbol{W}$ is defined in [10], which satisfies $\boldsymbol{I} = \boldsymbol{WI_C}$, and

$$\begin{cases} \boldsymbol{W^T K^T V^T D_x V K W} = \boldsymbol{M_x} \\ \boldsymbol{W^T K^T V^T D_y V K W} = \boldsymbol{M_y} \\ \boldsymbol{M_x} = \begin{bmatrix} 0 & 0.5 & 0 \\ 0.5 & 0 & 0 \\ 0 & 0 & 0 \end{bmatrix} \\ \boldsymbol{M_y} = \begin{bmatrix} 0 & 0 & 0.5 \\ 0 & 0 & 0 \\ 0.5 & 0 & 0 \end{bmatrix} \end{cases} \tag{14}$$

So the Equation (14) can be simplified to

$$\begin{cases} F_x = \frac{A}{2\mu_0} C_0 i_x \\ F_y = \frac{A}{2\mu_0} C_0 i_y \end{cases} \tag{15}$$

Usually, C_0 can be set as a constant to decouple and linearize the relationship of EMF and currents. However, there are constraints in magnetic bearings system, e.g. the magnetic field saturation due to magnetic material or the current saturation of power amplifier. Considering that inappropriate value of C_0 may lead to failure of outputting desired EMF due to the above constraints, how to optimize the bias current coefficient should be taken into consideration. We define two kinds of optimization objectives, (1) maximum electromagnetic force under the same structure and saturation constraints, and (2) minimum intensity of magnetic field under the same structure and EMF output.

3. Mathematical proofs of the optimal bias current coefficient

Assuming the area of each magnetic pole A, the number of turns of the coil N and the air gaps g_0 are the same, then we introduce them into Equations. (2), (5), (6), (11), can get Equation (16).

$$\boldsymbol{V} = \frac{u_0 N}{n g_0}\begin{bmatrix} n-1 & -1 & \cdots & -1 \\ -1 & n-1 & \ddots & \vdots \\ \vdots & \ddots & \ddots & -1 \\ -1 & \cdots & -1 & n-1 \end{bmatrix}_{n\times n} \tag{16}$$

Therefore, we can have

$$\begin{cases} \boldsymbol{V}^T\boldsymbol{D_x}\boldsymbol{V} = \frac{N^2\mu_0 A}{2n^2 g_0^2}\boldsymbol{L} \\ \qquad\qquad \cdot diag[\cos\theta_1 \quad \cos\theta_2 \quad \cdots \quad \cos\theta_n]\cdot\boldsymbol{L} \\ \boldsymbol{V}^T\boldsymbol{D_y}\boldsymbol{V} = \frac{N^2\mu_0 A}{2n^2 g_0^2}\boldsymbol{L} \\ \qquad\qquad \cdot diag[\sin\theta_1 \quad \sin\theta_2 \quad \cdots \quad \sin\theta_n]\cdot\boldsymbol{L} \\ \boldsymbol{L} = \begin{bmatrix} n-1 & -1 & \cdots & -1 \\ -1 & n-1 & \ddots & \vdots \\ \vdots & \ddots & \ddots & -1 \\ -1 & \cdots & -1 & n-1 \end{bmatrix}_{n\times n} \end{cases} \tag{17}$$

Define

$$\begin{cases} \boldsymbol{P_x} = \frac{2g_0^2}{N^2\mu_0 A}\boldsymbol{V}^T\boldsymbol{D_x}\boldsymbol{V} \\ \boldsymbol{P_y} = \frac{2g_0^2}{N^2\mu_0 A}\boldsymbol{V}^T\boldsymbol{D_y}\boldsymbol{V} \end{cases} \tag{18}$$

and introduce Equations (17) and (18) into Equation (14) to get Equation (19)

$$\begin{cases} \boldsymbol{W}^T\boldsymbol{K}^T\boldsymbol{P_x}\boldsymbol{K}\boldsymbol{W} = \frac{2g_0^2}{N^2\mu_0 A}\boldsymbol{M_x} \\ \boldsymbol{W}^T\boldsymbol{K}^T\boldsymbol{P_y}\boldsymbol{K}\boldsymbol{W} = \frac{2g_0^2}{N^2\mu_0 A}\boldsymbol{M_y} \end{cases} \tag{19}$$

The solution of the current-distribution matrix can be divided into two parts, one part is the solution matrix $\boldsymbol{W_{n\times 3}}$, which is only related to the number of magnetic poles and the corresponding angle of each magnetic pole; the other part is a scalar solution which is related to the structure parameters A,N,g_0 and μ_0 in Equation (20).

$$\boldsymbol{W} = \frac{\sqrt{2}g_0}{N\sqrt{\mu_0 A}}\boldsymbol{W_{n\times 3}} \tag{20}$$

From Equation (19), it can be seen that for a certain redundant structure, its parameters will become a part of the current-distribution matrix $\boldsymbol{W}$ by means of constant. However, $\boldsymbol{W}$determines the performance of the fault-tolerant control together with the bias current coefficient. Introduce Equation (15) into $\boldsymbol{I} = \boldsymbol{W}\boldsymbol{I_C}$ to get Equation (21).

$$\boldsymbol{I} = \boldsymbol{W}\cdot\begin{bmatrix} C_0 \\ F_x/C_0 \\ F_y/C_0 \end{bmatrix} \tag{21}$$

Define the general form of current-distribution matrix as in Equation (22), the current expression as Equation (23) can be derived by Equations (21) and (22).

$$\boldsymbol{W} = \begin{bmatrix} a_{11} & a_{12} & a_{13} \\ a_{21} & a_{22} & a_{23} \\ \vdots & \vdots & \vdots \\ a_{n1} & a_{n2} & a_{n3} \end{bmatrix} \tag{22}$$

$$\boldsymbol{I} = \begin{bmatrix} a_{11}C_0 + a_{12}\cdot\frac{F_x}{C_0} + a_{13}\cdot\frac{F_y}{C_0} \\ a_{21}C_0 + a_{22}\cdot\frac{F_x}{C_0} + a_{23}\cdot\frac{F_y}{C_0} \\ \vdots \\ a_{n1}C_0 + a_{n2}\cdot\frac{F_x}{C_0} + a_{n3}\cdot\frac{F_y}{C_0} \end{bmatrix} \tag{23}$$

The ith pole current can be expressed as

$$I_i = a_{i1}C_0 + a_{i2}\cdot\frac{F_x}{C_0} + a_{i3}\cdot\frac{F_y}{C_0}\ 0 < i \le n \tag{24}$$

As shown in Figure 2, we define

$$\vec{F} = F\angle\beta = F_x\cdot\vec{i} + F_y\cdot\vec{j} \tag{25}$$

Then Equation (24) can be expressed as

$$I_i = a_{i1}C_0 + \frac{F}{C_0}\cdot(a_{i2}\cos\beta + a_{i3}\sin\beta)\ 0 < i \le n \tag{26}$$

We define

$$\begin{cases} K_{i1} = a_{i1} \\ K_{i2} = a_{i2}\cos\beta + a_{i3}\sin\beta \end{cases} \tag{27}$$

Equation (24) can be simplified as

$$I_i = K_{i1}C_0 + \frac{K_{i2}F}{C_0}\ 0 < i \le n \tag{28}$$

Usually, $\boldsymbol{W}$ is obtained offline and stored in the FTCS, which means that K_{ij} is a constant for the any

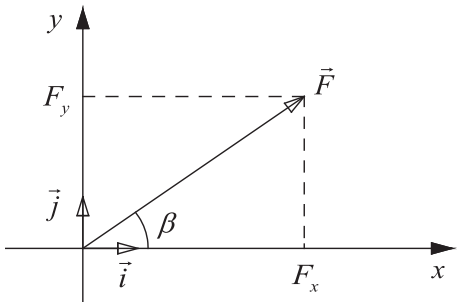

Figure 2. Exploitation of the desired force vector.

identified $\boldsymbol{W}$. Therefore, it can be known from Equation (28) that the value of C_0 directly affects the relationship between the desired EMF and the controlled current of each magnetic pole. the inappropriate value of C_0 will result in the inability to output the desired EMF because of saturation constraint. Moreover, there is an optimal value of C_0 in the any of following four conditions in Figure 3 from Equation (28), and the 4 conditions are from the combinations of K_{i1} and K_{i2} in Equation (27).

Obviously, the above ranges are symmetrical. In order to simplify the model, we only consider the positive value of C_0. Therefore the desired EMF can be generated only when $C_0 \in (C_3, C_4)$, where

$$\begin{cases} C_3 = \dfrac{\left|I_{\max} - \sqrt{I_{\max}^2 - 4K_{i1}K_{i2}\cdot F}\right|}{2|K_{i1}|} \\ C_4 = \dfrac{I_{\max} + \sqrt{I_{\max}^2 - 4K_{i1}K_{i2}\cdot F}}{2|K_{i1}|} \end{cases} \tag{29}$$

4. Optimization algorithms

4.1. Case A: Maximum electromagnetic force output under the same saturation constraints

Convert Equation (26) to Equation (30),

$$\left(C_0 - \frac{I_i}{2a_{i1}}\right)^2 + F\frac{(a_{i2}\cos\beta + a_{i3}\sin\beta)}{a_{i1}} = \frac{{I_i}^2}{4{a_{i1}}^2} \tag{30}$$

For any identified $\boldsymbol{W}$ and β, when I_i takes the maximum value, namely $I_{\max}$, an optimal value of bias current coefficient can be got as in Equation (31), so that

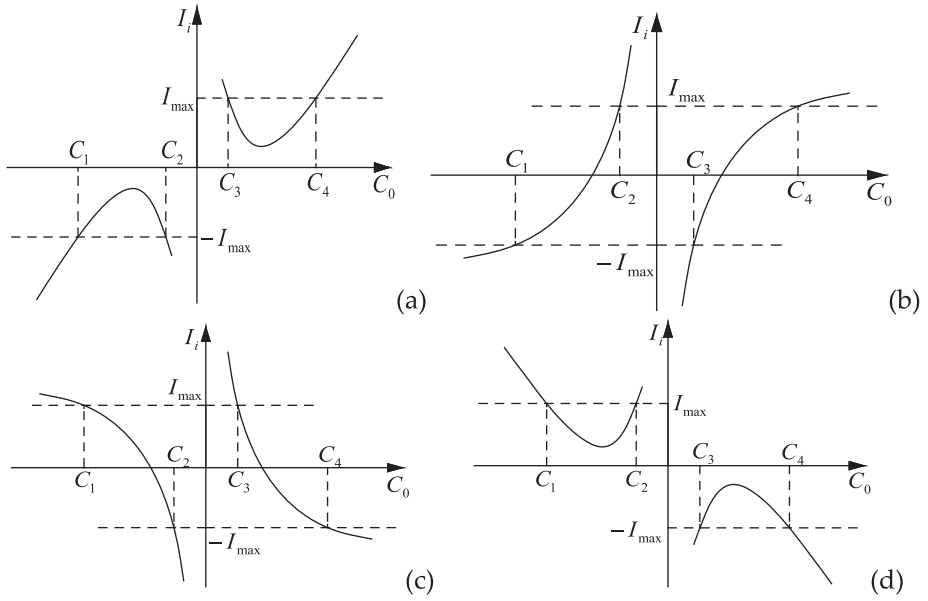

Figure 3. The ranges of C_0 under current saturation constraints. (a) $K_{i1} > 0, K_{i2} > 0$, (b) $K_{i1} > 0, K_{i2} < 0$, (c) $K_{i1} < 0, K_{i2} > 0$ and (d) $.K_{i1} < 0, K_{i2} < 0$.

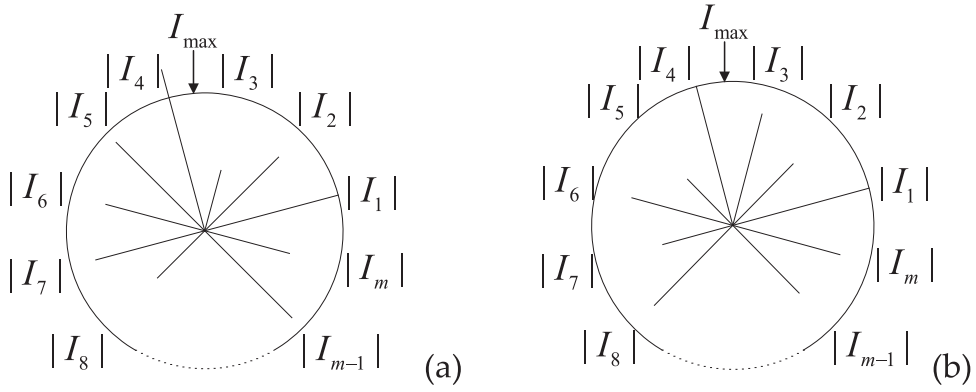

Figure 4. Current of every magnetic pole. (a) A magnetic pole current exceeds $I_{\max}$. (b) Two magnetic pole currents reach $I_{\max}$.

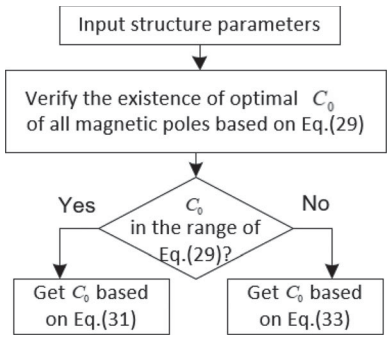

Figure 5. Flow chart of optimization algorithm for case A.

the corresponding structure can provide the maximum EMF.

$$C_0 = \frac{I_i}{2a_{i1}} \tag{31}$$

However, it is necessary to confirm whether the optimal C_0 satisfying Equation (31) exists within the range in Equation (29); if not, namely, when any magnetic pole current reaches the $I_{\max}$, there must be some other magnetic pole current exceeding the $I_{\max}$, as in Figure 4(a). This case means we cannot get the optimal C_0 from Equation (31), and need to consider that two magnetic pole currents reach the $I_{\max}$ at the same time, as in Figure 4(b). Assuming the q th and the p th magnetic pole current reach the $I_{\max}$ at the same time, the current expression is from Equation (32).

$$\begin{cases} I_{\max} = K_{p1}C_0 + \frac{K_{p2}F}{C_0} \\ I_{\max} = K_{q1}C_0 + \frac{K_{q2}F}{C_0} \end{cases} \tag{32}$$

The optimal value of C_0can be got from Equation (33).

$$\begin{cases} C_0 = \frac{(K_{q2}-K_{p2})I_{\max}}{K_{p1}K_{q2}-K_{q1}K_{p2}} \\ F = \frac{(K_{p1}-K_{q1})(K_{q2}-K_{p2})I_{\max}^2}{(K_{p1}K_{q2}-K_{q1}K_{p2})^2} \end{cases} \tag{33}$$

Figure 5 illustrates the flow chart of optimization algorithm for case A.

4.2. Case B: Minimum intensity of magnetic field under the same electromagnetic force output

From Equations (9), (11) and (21), the following Equation (34) can be obtained.

$$\boldsymbol{B} = \boldsymbol{V} \cdot \boldsymbol{W} \cdot \begin{bmatrix} C_0 \\ F_x/C_0 \\ F_y/C_0 \end{bmatrix} \tag{34}$$

Since the matrix $\boldsymbol{V}$ is determined by the structure parameters, we define $\boldsymbol{W'} = \boldsymbol{V} \cdot \boldsymbol{W}$, can have

$$\boldsymbol{B} = \boldsymbol{W'} \cdot \begin{bmatrix} C_0 \\ F_x/C_0 \\ F_y/C_0 \end{bmatrix} \tag{35}$$

Combined with Equation (28), we can have,

$$B_i = K_{i1}C_0 + \frac{K_{i2}F}{C_0} \quad 0 < i \le n \tag{36}$$

The relationship between the intensity of magnetic field and C_0 of each magnetic pole can be accurately obtained according to the matrix $\boldsymbol{V}$ and $\boldsymbol{W}$. Once the desired output EMF is generated, we need to find the optimal C_0 with the minimal value of the maximum intensity of magnetic field of all the poles, compared with other value of C_0. There are two cases, as shown in Figure 6.

In Figure 6(a), for the lowest point of the kth pole curve, when

$$C_0 = \sqrt{\left|\frac{K_{k2}F}{K_{k1}}\right|} \tag{37}$$

the magnetic flux intensity of a single magnetic pole can be taken to the minimum value of $B_k = 2\sqrt{K_{k1}K_{k2}F}$ or $B_k = 0$. In Figure 7(b), the lowest point is the intersection of the two curves, therefore the intensity of magnetic field expression corresponding to the sth and rth magnetic poles can be obtained from the Equation

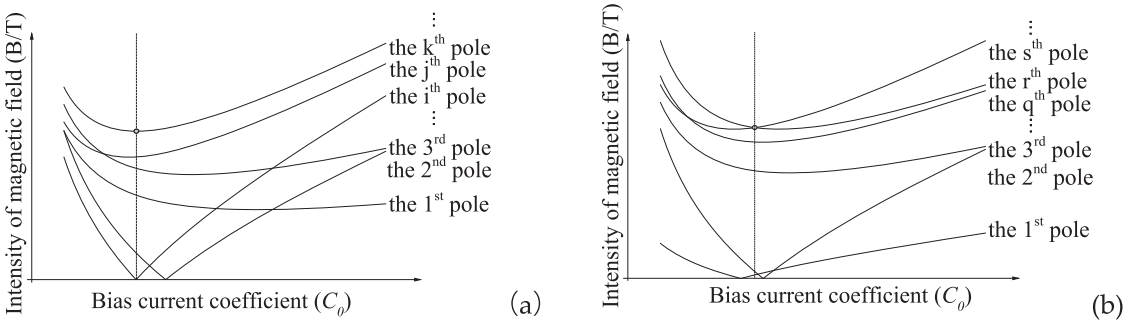

Figure 6. Intensity of magnetic field vs C_0 for all the poles. (a) The lowest point of maximum intensity of magnetic field is not the intersection of two curves. (b) The lowest point is the intersection of two curves.

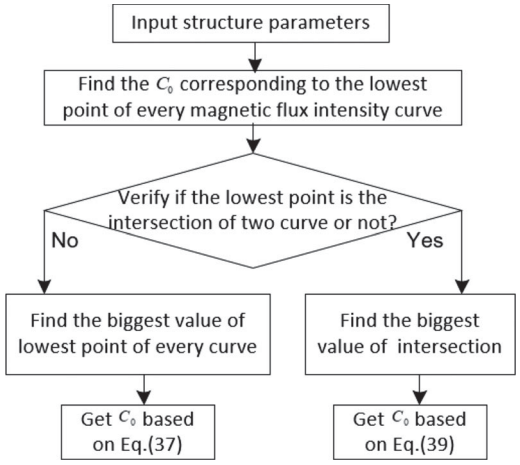

Figure 7. Flow chart of optimization algorithm for case B.

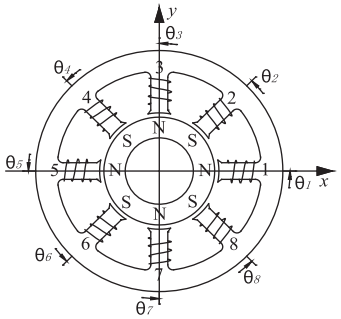

Figure 8. Octupole radial redundant structure.

(39).

$$B = \left|K_{s1}C_0 + \frac{K_{s2}F}{C_0}\right| = \left|K_{r1}C_0 + \frac{K_{r2}F}{C_0}\right| \tag{38}$$

The solution of Equation (38) is

$$\begin{cases} C_0 = \sqrt{\left|\frac{(K_{r2}-K_{s2})F}{(K_{s1}-K_{r1})}\right|} \\ B = |K_{s1}K_{r2} - K_{r1}K_{s2}|\sqrt{\left|\frac{F}{(K_{s1}-K_{r1})(K_{r2}-K_{s2})}\right|} \end{cases} \tag{39}$$

Flow chart of optimization algorithm for case B is in Figure 7, it is obvious that the optimal C_0 can always be got from one of the Equations (31), (33), (37) and (39).

5. Numerical verification

By taking an 8-pole symmetrical radial magnetic bearing as an example, its structure is shown in Figure 8 and parameters are presented in Table 1.

Based on Equation (5), we can have Equation (40) for this example.

$$\boldsymbol{R} = \frac{g_0}{u_0 A} \cdot \begin{bmatrix} 1 & -1 & 0 & \cdots & 0 \\ 0 & 1 & -1 & \ddots & \vdots \\ \vdots & 0 & \ddots & \ddots & 0 \\ 0 & \cdots & 0 & 1 & -1 \\ 1 & 1 & \cdots & 1 & 1 \end{bmatrix}_{8\times 8} \tag{40}$$

By introducing the structure parameters into Equation (18), we can have

$$\begin{cases} \boldsymbol{P_x} = \frac{\sqrt{2}}{16} \cdot \begin{bmatrix} 6\sqrt{2} & -1-\sqrt{2} & -\sqrt{2} & 1-\sqrt{2} & 0 & 1-\sqrt{2} & -\sqrt{2} & -1-\sqrt{2} \\ -1-\sqrt{2} & 6 & -1 & 0 & \sqrt{2}-1 & 0 & -1 & -2 \\ -\sqrt{2} & -1 & 0 & 1 & \sqrt{2} & 1 & 0 & -1 \\ 1-\sqrt{2} & 0 & 1 & -6 & 1+\sqrt{2} & 2 & 1 & 0 \\ 0 & \sqrt{2}-1 & \sqrt{2} & 1+\sqrt{2} & -6\sqrt{2} & 1+\sqrt{2} & \sqrt{2} & \sqrt{2}-1 \\ 1-\sqrt{2} & 0 & 1 & 2 & 1+\sqrt{2} & -6 & 1 & 0 \\ -\sqrt{2} & -1 & 0 & 1 & \sqrt{2} & 1 & 0 & -1 \\ -1-\sqrt{2} & -2 & -1 & 0 & \sqrt{2}-1 & 0 & -1 & 6 \end{bmatrix} \\ \boldsymbol{P_y} = \frac{\sqrt{2}}{16} \cdot \begin{bmatrix} 0 & -1 & -\sqrt{2} & -1 & 0 & 1 & \sqrt{2} & 1 \\ -1 & 6 & -1-\sqrt{2} & -2 & -1 & 0 & \sqrt{2}-1 & 0 \\ -\sqrt{2} & -1-\sqrt{2} & 6\sqrt{2} & -1-\sqrt{2} & -\sqrt{2} & 1-\sqrt{2} & 0 & 1-\sqrt{2} \\ -1 & -2 & -1-\sqrt{2} & 6 & -1 & 0 & \sqrt{2}-1 & 0 \\ 0 & -1 & -\sqrt{2} & -1 & 0 & 1 & \sqrt{2} & 1 \\ 1 & 0 & 1-\sqrt{2} & 0 & 1 & -6 & 1+\sqrt{2} & 2 \\ \sqrt{2} & \sqrt{2}-1 & 0 & \sqrt{2}-1 & \sqrt{2} & 1+\sqrt{2} & -6\sqrt{2} & 1+\sqrt{2} \\ 1 & 0 & 1-\sqrt{2} & 0 & 1 & 2 & 1+\sqrt{2} & -6 \end{bmatrix} \end{cases} \tag{41}$$

Table 1. Parameters of the structure in Figure 8.

Parameter	Value	Unit
Number of circles, N	200	–
Air gap, g_0	10^{-4}	m
Saturation current, I_{max}	5	A
Pole angle, θ	45	degree
Pole area, A	491	mm^2
Intensity of magnetic saturation, B_{max}	1.2	T

Table 2. Computational cost of the proposed algorithm.

Case	Value	Unit
A	6.6	us
B	52.8	us

We can find one solution of $\boldsymbol{W}$ in Equation (42) from [10], with identity matrix $\boldsymbol{K}$. Obviously, the structure parameters of the magnetic bearing are contained in $\boldsymbol{W}$, as constants.

$$\boldsymbol{W} = \frac{g_0}{4N\sqrt{\mu_0 A}} \begin{bmatrix} 2 & 2 & 0 \\ -2 & -\sqrt{2} & -\sqrt{2} \\ 2 & 0 & 2 \\ -2 & \sqrt{2} & -\sqrt{2} \\ 2 & -2 & 0 \\ -2 & \sqrt{2} & \sqrt{2} \\ 2 & 0 & -2 \\ -2 & -\sqrt{2} & \sqrt{2} \end{bmatrix} \tag{42}$$

The computational cost of the proposed algorithm of different cases is shown in Table 2; the values are measured by CCS Profile clock when the proposed algorithm is running in the TMS320F28335 DSP with the core clock of 150 MHz.

5.1. Maximum EMF output

Firstly, we consider the condition of no failed actuator. Figure 9(a) illustrates the maximum output EMF under variable I_{max}; Figure 9(b) describes the relationship between the C_0 and the maximum *EMF* output when I_{max} is 5 A. we can find the optimal C_0 in Equation (43) based on the proposed approach.

$$\begin{cases} C_0 = I_1/2a_{11} = 24.8397 \\ F = 617.0088 \end{cases} \tag{43}$$

Figures 10–11 illustrates the same relationships when the 8th actuator fails, and the $\boldsymbol{W}$ for this condition is shown in Equation (44).

$$\boldsymbol{W} = \begin{bmatrix} 0.2013 & 0.1718 & -0.0712 \\ 0 & 0 & -0.1423 \\ 0.2013 & 0.0712 & 0.0295 \\ 0 & 0.1423 & -0.1423 \\ 0.2013 & -0.0295 & -0.0712 \\ 0 & 0.1423 & 0 \\ 0.2013 & 0.0712 & 0.1718 \\ 0 & 0 & 0 \end{bmatrix} \tag{44}$$

5.2. Minimum intensity of magnetic field

When expected EMF is $\begin{bmatrix} F_x & F_y \end{bmatrix} = \begin{bmatrix} 500\,\boldsymbol{N} & 0\,\boldsymbol{N} \end{bmatrix}$, we can find the optimal solution C_0, considering two same failure condition based on the proposed approach, (1) no failed actuator, $C_0 = 22.3607$, and $B_{max} = 1.13$ T; (2) the 8th actuator fails, $C_0 = 22.3593$, and $B_{max} = 1.13$ T.

5.3. Performance simulations of FTC adopting proposed optimization algorithms

The proposed optimization algorithms can help to find the optimal C_0 in the FTC of magnetic bearing. The implementation details of FTC of magnetic bearings can be found in [10–12,14,21]. To verify the effectiveness of the proposed optimization approach, the simulations based on Matlab/Simulink was carried on. The structure and parameters of magnetic bearing are in Figure 8 and Table 1, respectively.

As in Figure 12(a), curve B demonstrates the trajectory of rotor when the optimized $C_0 = 23$ is chosen. The failure conditions were designed as follows. (1) at 0.5 s, the rotor was suspended near its equilibrium position (0.001 m); (2) the 8th coil failed at 1 s; (3) then the 6th coil failed at 1.5 s. It is obvious that the can return to the equilibrium position after the failures of coils because the supporting structure was reconfigured under the FTC. Figure 12(b) describes the electromagnetic force in the reconfiguration, it is clear that the output electromagnetic force (curve D) can compensate the disturbances in the reconfiguration to maintain the resultant force (curve C) near the 0 N. The trajectories of rotor (curve A and B) are similar if ignoring the reconfiguration, it means that whether or not the optimal C_0 is chosen, the performance of FTC in this case is similar to effectively deal with the failure of coils.

Figure 13 demonstrates different performances if a sinusoidal disturbance with the magnitude of $\pm$ 300 N and frequency of 100 rad/s is added into the control loop. The optimized C_0 chosen in FTC can effectively compensate the disturbance(in curve B) compared with the case in curve A, it means that the optimized C_0 can effectively add the EMF output capacity if the extreme cases occur. Moreover, the real-time performance of FTC will have the decisive effects to maintain the stability of rotor in the reconfiguration if some coils fail.

5.4. Versatility

To prove the versatility of proposed approach, a different redundant structure in Figure 14 is chosen, while the parameters are in Table 3. A matrix $\boldsymbol{W}$ for this

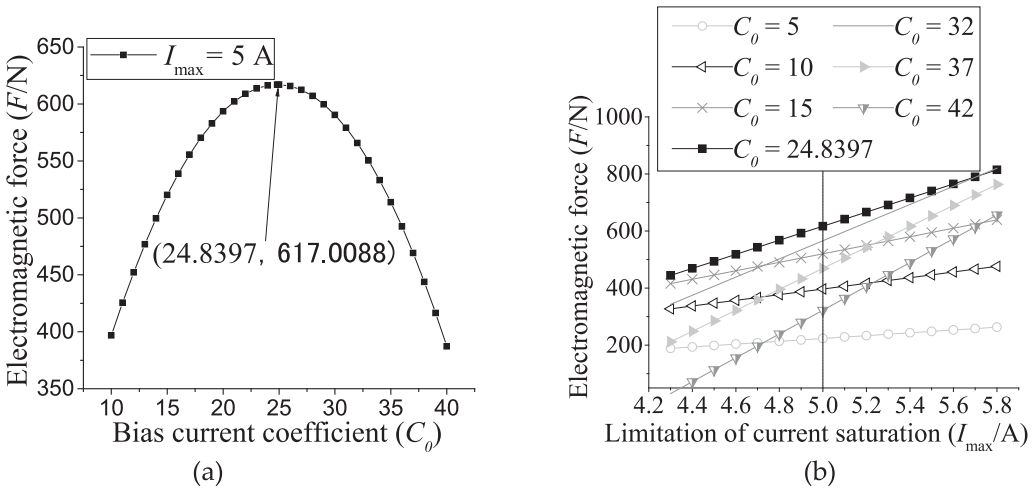

Figure 9. (a) Maximum EMF vs C_0 when I_{max} is 5 A. (b) Maximum EMF vs I_{max}.

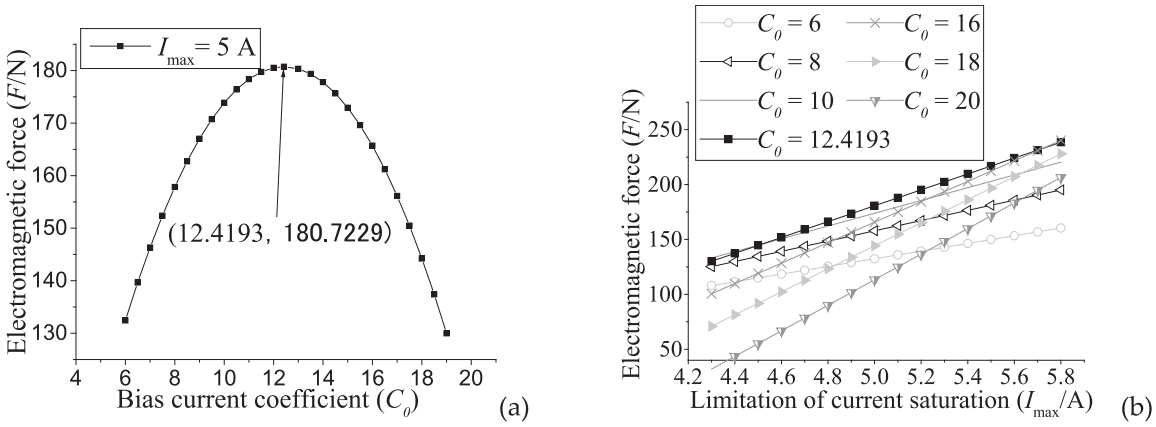

Figure 10. When the 8th actuator fails, the curves of (a) Maximum EMF vs C_0, and (b) Maximum EMF vs I_{max}.

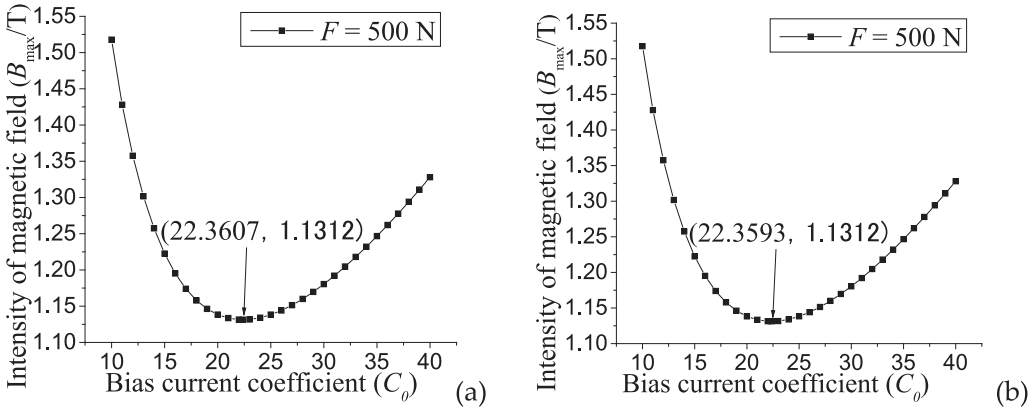

Figure 11. B_{max} vs C_0 under the condition of (a) no failed actuator, and (b) the 8th actuator fails.

structure can be got in Equation (45).

$$\boldsymbol{W} = \begin{bmatrix} 0.3932 & 0.2241 & 0 \\ -0.3932 & -0.1691 & -0.2241 \\ 0.3932 & -0.1691 & 0.2241 \\ -0.3932 & 0.2241 & 0 \\ 0.3932 & -0.1691 & -0.2241 \\ -0.3932 & -0.1691 & 0.2241 \end{bmatrix} \tag{45}$$

Figures 15 and 16 illustrate the similar results as in Figures 10 and 11 for the 6-pole structure in Figure 14. It can be seen that the optimal C_0 can be got based on the discussed approach even for this 6-pole structure, which means the good versatility of the discussed approach.

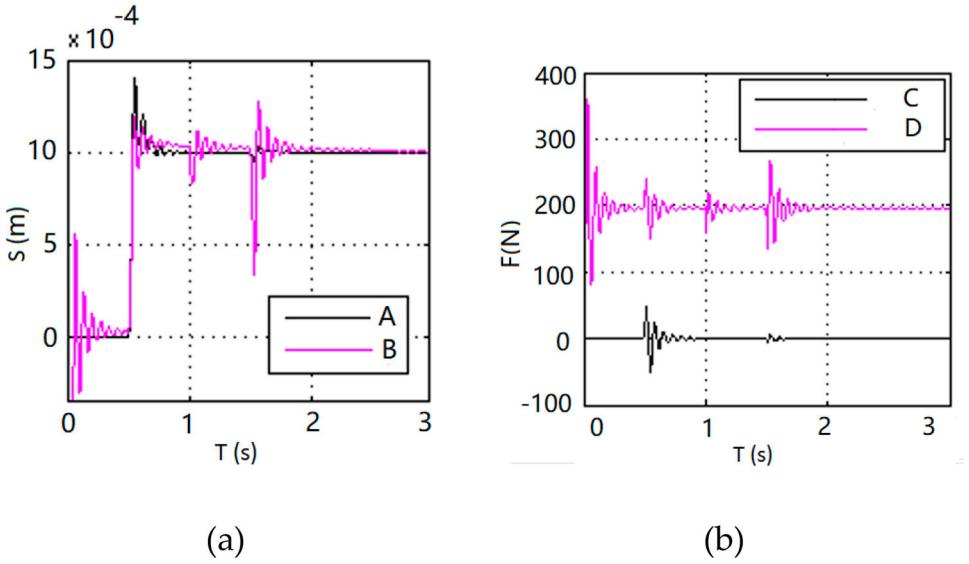

Figure 12. Simulation results of FTC, (a) trajectory of rotor, A-a random selection, $C_0 = 7$, B-the optimized $C_0 = 23$. (b) EMF in the reconfiguration, C-resultant force, D-the output EMF.

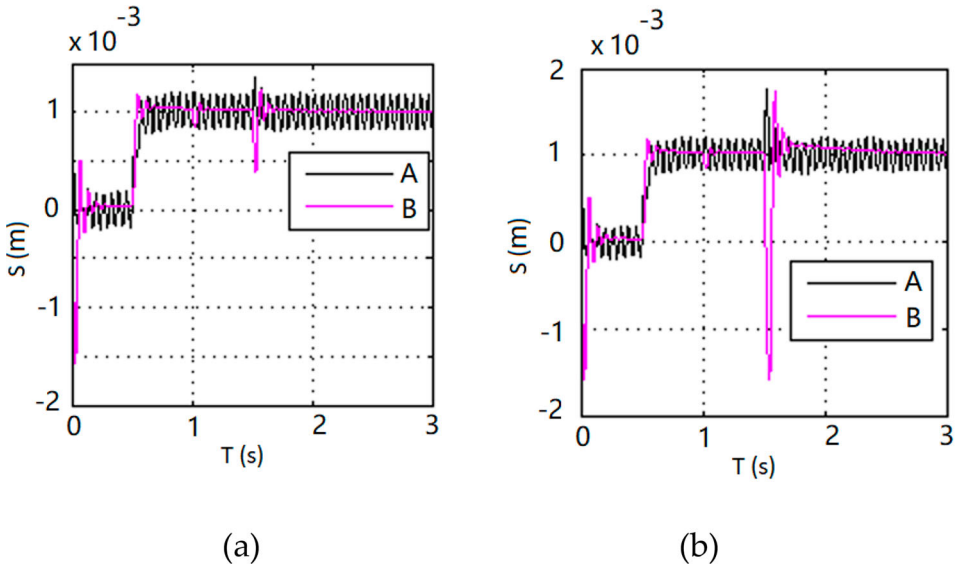

Figure 13. Simulation results of FTC. Trajectory of rotor in the reconfiguration time of 1 ms (a) and 10 ms (b), under a sinusoidal disturbance, the magnitude of ± 300 N and frequency of 100 rad/s. A-a random selection, $C_0 = 7$, B-the optimized $C_0 = 23$.

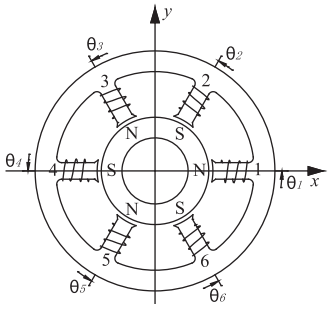

Figure 14. Another 6-pole redundant supporting structure.

Table 3. Parameters of the structure in Figure. 14.

Parameter	Value	Unit
Number of circles, N	85	–
Air gap, g_0	4×10^{-4}	m
Saturation current, I_{max}	5	A
Pole angle, θ	60	degree
Pole area, A	57	mm^2
Intensity of magnetic field saturation, B_{max}	1.2	T

6. Conclusions

Aiming at the FTC of active magnetic bearings, this paper proposes optimization approaches of bias current coefficient based on structure parameters. The relevant conclusions are as follows,

(1) For a certain structure, there is an optimal C_0, and only when the bias current coefficient is within a certain range, the desired EMF can be generated. This paper proves the existence of the range.
(2) To the two kinds of optimization objectives, (a) maximum EMF under the same structure and

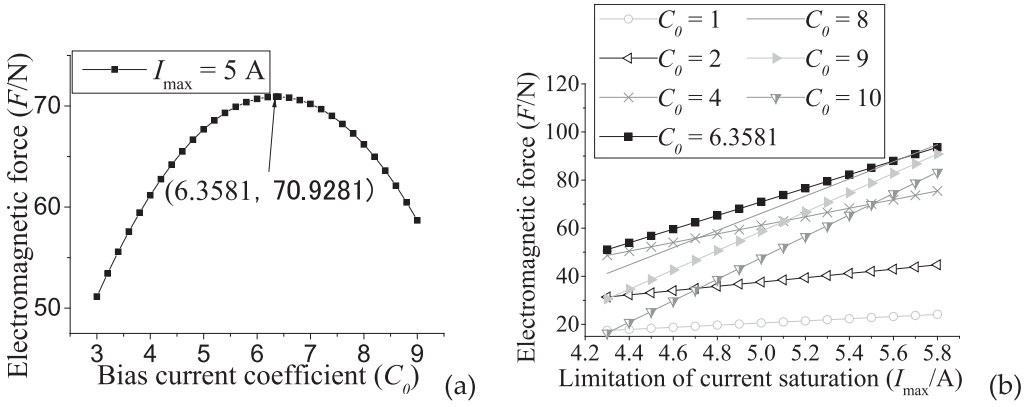

Figure 15. (a) Maximum electromagnetic force vs C_0. (b) Maximum electromagnetic force vs Imax, for the structure in Figure 14.

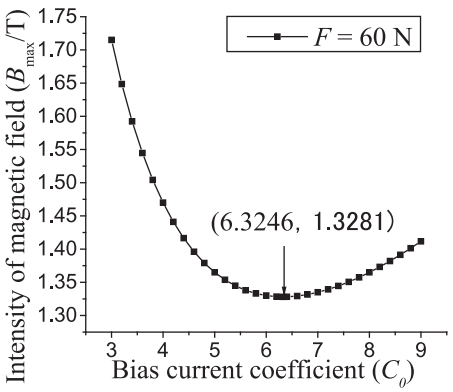

Figure 16. B_{max} vs C_0 for the structure in Figure 14.

saturation constraints and (b) minim intensity of magnetic field under the same structure and EMF output, we design effective optimization algorithms to find the optimal solution of C_0. In addition, the versatility of proposed approaches has been proved.

The limitation of the proposed approach is that the basic electromagnetic force linearization theory is based on the assumption, namely, the solution of Equation (14) must consider the constraints in the actual applications, as follows: (1) the saturation of magnetic field; (2) the saturation of current in the power amplifier; (3) the redundancy of the magnetic bearings – the more redundant coils, the more failed ones allowed; (4) the ratio of maxim EMF required and EMF designed; (5) the rotor dynamics required or precision; (6) the failed coils are continuously or discretely arranged.

The future work should focus on the optimization approach of bias current coefficient under certain constraints, and the size of the redundancy required for certain types of faults.

Acknowledgements

This work was supported National Natural Science Funds of China under Grants 51575411, the National Key Program of China under Grant No. 2018YFB2000103 and the Fundamental Research Funds for the Central Universities of China under Grants 2020-YB-022 and WUT2019III143CG.

Methodology, Xin Cheng; Validation, Meiqian Lu and Shuai Deng; Writing – original draft preparation, Meiqian Lu; Writing – review and editing, Baixin Cheng; supervision, Rougang Zhou.

Disclosure statement

No potential conflict of interest was reported by the authors.

Funding

This work was supported National Natural Science Funds of China under Grants [51575411], the National Key Program of China under [Grant No. 2018YFB2000103] and the Fundamental Research Funds for the Central Universities of China under Grants [2020-YB-022 and WUT2019III143CG].

References

[1] Aenis M, Knopf E, Nordmann R. Active magnetic bearings for the identification and fault diagnosis in turbomachinery. Mechatronics. 2002;12(8):1011–1021.

[2] Cheng X, Zhang L, Zhou RG, et al. Analysis of output precision characteristics of digital switching power amplifier in active magnetic bearing system. Automatika. 2017;58(2):205–215.

[3] Aanstoos TA, Kajs JP, Brinkman WG, et al. High Voltage Stator for a Flywheel Energy Storage System. IEEE Trans Magn. 2001;37(1):242–247.

[4] Cheng X, Wang B, Chen Q, et al. A unified design and the current ripple characteristic analysis of digital switching power amplifier in active magnetic-levitated bearings. *Int J Appl Elect Mech*. 2017;55:391–407.

[5] Schweitzer G, Maslen EH. Magnetic bearings: theory, design, and application to rotating machinery. Berlin: Springer; 2009. ch. 14, pp. 407–433.

[6] Arslan AA, Khalid M-H. Advanced fault tolerant air-fuel ratio control of internal combustion gas engine for sensor and actuator faults. IEEE Access. 2019;7:17634–17643.

[7] Hudson S, Sundar RSS, Koppu S. Fault control using triple modular redundancy (TMR), in progress in computing, analytics and networking. Singapore: Springer; 2018. pp. 471–480.

[8] Cheng X, Chen Q, Zeng H, et al. Reconfiguration rules for loosely-coupled redundant supporting structure in radial magnetic bearings. Int J Appl Elect Mechan. 2016;51(2):91–106.
[9] Cheng X, Cheng B, Lu M, et al. An online fault-diagnosis of electromagnetic actuator based on variation characteristics of load current. Automatika. 2020;61:11–20.
[10] Maslen EH, Meeker DC. Fault tolerance of magnetic bearings by generalized bias current linearization. IEEE Trans Magn. 1995;31(3):2304–2314.
[11] Na UJ, Palazzolo AB. Optimized realization of fault-tolerant heteropolar magnetic bearings. J Vib Acoust-trans ASME. 2000;122:209–221.
[12] Na UJ, Palazzolo AB, Provenza A. Test and theory correlation study for a flexible rotor on fault-tolerant magnetic bearings. J VibAcoust, Trans ASME. 2002;124:359–366.
[13] Li MH, Palazzolo A, Kennyetal A. Fault-tolerant homopolar magnetic bearings. IEEE Trans Magn. 2004;40(5):3308–3318.
[14] Noh MD, Cho S-R, Kyung J-H, et al. Design and implementation of a fault-tolerant magnetic bearing system for Turbo-Molecular Vacuum Pump. IEEE-ASME Trans Mechatron. 2005;10:626–631.
[15] Meeker DC, Maslen EH, Noh MD. An augmented circuit model for magnetic bearings including eddy currents, fringing and leakage. IEEE Trans Magn. 1996;32:3219–3227.
[16] Na UJ, Palazzolo AB. Fault tolerance of magnetic bearings with material path reluctances and fringing factors. IEEE Trans Magn. 2000;36:3939–3946.
[17] Arslan AA, Khalid M-H. A review of fault tolerant control systems: advancements and applications. Measurement. 2019;143:58–68.
[18] Alwi H, Edwards C, Tan CP. Fault tolerant control and fault detection and isolation. Fault Detect. Fault-Toler. Control Using Sliding Modes, Springer-Verlag, London, 2011, 7–27.
[19] Wang Y, Donghua Zhou S, Qin J, et al. Active fault-tolerant control for a class of nonlinear systems with sensor faults. Int J Control Autom Syst. 2008;6:339–350.
[20] Yang F, Zhang H, Jiang B, et al. Adaptive reconfigurable control of systems with time-varying delay against unknown actuator faults. Int J Adapt Control Signal Process. 2014;8:1206–1226. doi:10.1002/acs.2439.
[21] Arslan AA, Khalid M-H. Hybrid fault tolerant control for air–fuel ratio control of internal combustion gasoline engine using Kalman filters with advanced redundancy. Meas control. 2019;52(5–6):473–492.
[22] Arslan AA, Khalid M-H. Robust active fault-tolerant control for internal combustion gas engine for air–fuel ratio control with statistical regression-based observer model. Meas Control. 2019;52:1179–1194.
[23] Na UJ, Palazzolo AB. The fault-tolerant control of magnetic bearings with reduced controller outputs. J Dyn Syst, Meas Control-trans ASME. 2001;123:219–224.
[24] Cheng X, Cheng BX, Liu H, et al. An accurate linearization of electromagnetic force of heteropolar magnetic bearings with redundant structures. J Eng Gas Turbines Power, Trans ASME. 2020. DOI:10.1115/1.4046703
[25] Cheng X, Liu H, Song S, et al. Reconfiguration of tightly-coupled redundant supporting structure in active magnetic bearings under the failures of electromagnetic actuators. Int J Appl Electromagn Mech. 2017;54:421–432.